



Wiley Analytical Science Virtual Conference, 2021

20 April | 4pm-5pm CEST

Correlative Raman & SEM Imaging: Current Trends and Applications

Both Raman and SEM imaging are very well-established techniques in material research and geosciences. This virtual seminar will provide an introduction to basic principles of both techniques and their use in combination. Novel and innovative application examples from different fields of research will be presented to demonstrate the advantages of the correlative approach.

Key learnings:

- How to integrate Raman and SEM into one instrument
- How to differentiate materials with the same elemental composition
- Applications from materials and earth sciences requiring correlative, nondestructive analysis techniques for their full characterization
- The basics of confocal Raman and SEM imaging

Register here

Sponsored by



Wiley Analytical Science

Microscopic melanoma detection and classification: A framework of pixel-based fusion and multilevel features reduction

Amjad Rehman¹ | Muhammad A. Khan²  | Zahid Mehmood³  | Tanzila Saba¹  |
 Muhammad Sardaraz⁴ | Muhammad Rashid⁵

¹Artificial Intelligence and Data Analytics (AIDA) Lab, CCIS Prince Sultan University, Riyadh, Saudi Arabia

²Department of CS&E, HITEC University, Taxila, Pakistan

³Department of Computer Engineering, University of Engineering and Technology, Taxila, Pakistan

⁴Department of Computer Science, COMSATS University Islamabad, Attock, Pakistan

⁵Department of Computer Engineering, Umm Al-Qura University, Makkah, Saudi Arabia

Correspondence

Tanzila Saba, Artificial Intelligence and Data Analytics (AIDA) Lab, CCIS Prince Sultan University, Riyadh 11586, Saudi Arabia.
 Email: drstanzila@gmail.com

Funding information

Prince Sultan University Riyadh KSA, Grant/Award Number: RG-CCIS-2017-06-02

Review Editor: George Perry

Abstract

The numbers of diagnosed patients by melanoma are drastic and contribute more deaths annually among young peoples. An approximately 192,310 new cases of skin cancer are diagnosed in 2019, which shows the importance of automated systems for the diagnosis process. Accordingly, this article presents an automated method for skin lesions detection and recognition using pixel-based seed segmented images fusion and multilevel features reduction. The proposed method involves four key steps: (a) mean-based function is implemented and fed input to top-hat and bottom-hat filters which later fused for contrast stretching, (b) seed region growing and graph-cut method-based lesion segmentation and fused both segmented lesions through pixel-based fusion, (c) multilevel features such as histogram oriented gradient (HOG), speeded up robust features (SURF), and color are extracted and simple concatenation is performed, and (d) finally variance precise entropy-based features reduction and classification through SVM via cubic kernel function. Two different experiments are performed for the evaluation of this method. The segmentation performance is evaluated on PH2, ISBI2016, and ISIC2017 with an accuracy of 95.86, 94.79, and 94.92%, respectively. The classification performance is evaluated on PH2 and ISBI2016 dataset with an accuracy of 98.20 and 95.42%, respectively. The results of the proposed automated systems are outstanding as compared to the current techniques reported in state of art, which demonstrate the validity of the proposed method.

KEY WORDS

classification, contrast stretching, feature reduction, lesions segmentation, skin cancer

1 | INTRODUCTION

The number of diagnosed patients with skin cancer is increased drastically from the last few years (Afza, Khan, Sharif, & Rehman, 2019; Pathan, Prabhu, & Siddalingaswamy, 2019). Two major types of skin cancer exist: melanoma and benign (Khan et al., 2018; Saba, Khan, Rehman, & Marie-Sainte, 2019). Among all skin cancer types, melanoma is one of the deadliest that contributes more deaths annually among young peoples. In the United States, during 2019, approximately 192,310

new cases of melanoma are diagnosed whose increased rate is 7.7%. The number of deaths that occurred in 2019 by melanoma is 7,230 (4,740 men and 2,490 women) (Cancer Facts and Figures, 2019). The survival rate of melanoma will be reduced, and it is curable if it is diagnosed at an early stage (Nasir et al., 2018). However, the manual diagnosis procedure demands well-trained dermatologist experts. The well-trained dermatologist required a huge cost and time. Therefore, a consistent automated system is needed to increase the performance of dermatologist by employing less effort (Akram, Khan, Sharif, & Yasmin,

2018; Majtner, Yildirim-Yayilgan, & Hardeberg, 2019; Saba, 2019; Yousaf et al., 2019).

The more recent, various computerized methods are presented for detection and recognition of melanoma using dermoscopy data (Majumder & Ullah, 2019; Seelatha, Subramanyam, & Prasad, 2019). Through dermoscopy, the skin images are captured, which gives more clarity of lesion spots. But still, several challenges exist which decreased the accuracies of these automated systems. In general, a simple automated system follows these steps: preprocessing of original data, detection of the lesion through segmentation or features-based techniques, and finally classification by extracting patterns information (Jadooki, Mohamad, Saba, Almazyad, & Rehman, 2016; Majumder & Ullah, 2019; Marka, Carter, Toto, & Hassanpour, 2019; Sharif et al., 2017). A lot of techniques are presented for contrast enhancement in this domain to improve the visual quality of lesion in the given images. Moreover, a few well-known segmentation methods available in computer vision are thresholding, K-means, Fuzzy-C means, and saliency (Khan, Lali, et al., 2019; Khan, Rashid, Sharif, Javed, & Akram, 2019; Safdar et al., 2019). The famous feature extraction techniques which are used for classification are ABCDE, HOG, point, texture, geometric, and many more (Ebrahim, Kolivand, Rehman, Rahim, & Saba, 2018; Sadad, Munir, Saba, & Hussain, 2018). The classification algorithms such as SVM, KNN, neural network, and decision trees are utilized for features classification (Jianu, Ichim, & Popescu, 2019; Pathan, Aggarwal, Prabhu, & Siddalingaswamy, 2019).

The most crucial problem is the low contrast skin lesion images. The low contrast lesion images affect the segmentation performance due to the similarity between healthy and infected lesion areas. The second major issue is lesion detection through segmentation techniques because the lesions are irregular and different shapes, so a consistent technique is required. The third issue of these automated systems is the classification of benign and melanoma lesions because a huge color similarity exists among lesion types. In this article, we consider three major problems that decline the recognition performance of an automated system. Such kinds of problems are low contrast lesions, irregular lesion segmentation, and reduction of vague features. To deal with these challenges, we propose an automated method based on classical features extraction and higher variance precise entropy (VpE)-based features reduction. The major contributions of this article are as follows:

1. A mean-based contrast stretching function is proposed and feeds its output to top-hat and bottom-hat filters individually. Later, fuse the output of both filters using a subtraction approach.
2. Parallel via maximum probability mass function (PvMPMF) is introduced for a fusion of seed region growing (SRG) and graph cut-based segmented images.
3. Multilevel features (i.e., SURF, HOG, and color) are concatenated and reduced irrelevant features through a VpE method.

Further, this article is organized into four main sections: Section 2 presents state of art in depth; Section 3 comprises detailed proposed research framework for microscopic melanoma detection, classification;

Section 4 exhibits results; and Section 5 concludes the main findings of the study.

2 | RELATED WORK

In medical image analysis, various methods are introduced to diagnose and cure chronic diseases (Abbas et al., 2018; Abbas, Saba, Rehman, Mehmood, Javaid, et al. 2019; Abbas, Saba, Rehman, Mehmood, Kolivand, et al. 2019; Amin et al., 2019; Amin, Sharif, Yasmin, Saba, & Raza, 2019; Jamal, Hazim Alkawaz, Rehman, & Saba, 2017; Mughal, Muhammad, Sharif, Saba, & Rehman, 2017; Mughal, Sharif, Muhammad, & Saba, 2017; Mughal, Muhammad, Sharif, Rehman, & Saba, 2018; Ullah et al., 2019; Saba, 2020). Accordingly, several in-depth techniques/reviews are presented (Javed, Rahim, Saba, & Rehman, 2020; Norouzi et al., 2014; Saba, Bokhari, Sharif, Yasmin, & Raza, 2018; Saba, Rehman, Mehmood, Kolivand, & Sharif, 2018), and automated systems are developed in state of art (Saba et al., 2019; Saba, Al-Zahrani, & Rehman, 2012; Rehman, Abbas, Saba, Mahmood, & Kolivand, 2018; Rehman, Abbas, Saba, Mehmood, et al., 2018; Rehman, Abbas, Saba, Rahman, et al., 2018; Rahim, Norouzi, Rehman, & Saba, 2017; Rahim, Rehman, Kurniawan, & Saba, 2017; Iftikhar, Fatima, Rehman, Almazyad, & Saba, 2017; Fahad et al., 2018). However, among all, detection of lesions from dermoscopy images is a challenging task from the last few years, and various techniques are developed by several researchers using computer vision (CV) and machine learning (Amin, Sharif, Yasmin, Saba, & Raza, 2019; Amin et al., 2019; Husham, Alkawaz, Saba, Rehman, & Alghamdi, 2016; Iqbal et al., 2019; Iqbal, Ghani, Saba, & Rehman, 2018; Iqbal, Khan, Saba, & Rehman, 2017; Jamal et al., 2017; Fahad et al., 2018). Pathan, Prabhu, and Siddalingaswamy (2018) developed a novel hair detection and segmentation method by utilizing specific properties of the lesion. Their work is composed of two parts. First, a new hair detection method is introduced by utilizing 2D directional Gabor filters. Second, a geometric model based on chrominance is utilized to distinguish between the lesion and normal skin accurately. Chrominance properties are used to incorporate the speed function to stop evaluation at the lesion boundary. Filali and Belkadi (2019) presented a contrast-based method for skin lesion segmentation. First, the image was decomposed into superpixels and then used a regional similarity to compute the regional background connectivity and estimate the regional contrast. Then feature weighting technique is utilized for contrast accuracy. A hierarchical inference technique is used to deal with scale variation of lesions. Khan et al. (2018) introduced a novel lesion detection and classification technique based on probabilistic distribution segmentation and controlled entropy-based feature selection. The results are using two segmentation techniques: uniform distribution and normal distribution, which are fused and get the final segmented region. Then multilevel features were extracted and selected under controlled conditional-based entropy environment. Finally, the lesion is classified into multiple categories by using a multiclass support vector machine. Akram et al. (2018) presented an improved segmentation and feature selection method for lesions segmentation and recognition. The presented method comprises the threefold contribution. First, they exploited the three-color spaces to extract the foreground from the background.

Second, they segment the lesion area based on the best-extended texture features. Third, they introduce the improved feature extraction and selection method based on the neighborhood component analysis.

Recently, Khan, Akram, Sharif, Javed, et al. (2019) and Khan, Akram, Sharif, Saba, et al. (2019) presented another efficient framework for accurate lesion segmentation and classification. They improve the contrast of the lesion as compared to the skin area so that the overall segmentation accuracy can be improved. A saliency map is constructed from an enhanced 2D blue channel, and then a threshold function is applied, which produces the binary image. Then the particle swarm optimization is utilized for refinement and detection of the lesion border. Feature selections are made by using a genetic algorithm and classify the lesion by using SVM. Sengupta, Mittal, and Modi (2019) presented an improved lesion segmentation method. First, a three-stage preprocessing approach, which comprised contrast enhancement, color space conversion, and filtering, is applied. Then, three conventional edge detection techniques, Sobel, Prewitt, and Canny, are used to obtain the edge map of the lesion. Finally, ant colony optimization is utilized to get the improved edge contour. Dalila, Zohra, Reda, and Hocine (2017) presented an ant colony-based segmentation method, which takes the three types of features such as textural, geometrical, and colors into consideration. The prime objective of their work is to evaluate the efficiency of the presented lesion segmentation method and extract the most distinctive feature that discriminates the melanoma from benign.

Majumder and Ullah (2019) presented the novel and effective features related to size, color, and shape of the lesion based on the ABCD rule. They implement a two-stage segmentation method including Chan-Vese and Otsu algorithm. The Dull Razor is used to remove dark and black hair from images. Finally, an artificial neural network is applied as a classifier. Their result shows significant improvement as compared to existing techniques.

3 | PROPOSED METHOD

The proposed automated skin lesion detection and classification system follows the sequence of filters: fusion-based contrast stretching, graph-cut via SRG-based segmentation, concatenation of multilevel features, and reduction of less informative features. The flow of the proposed automated system is depicted in Figure 1.

3.1 | Contrast stretching

Contrast stretching is a very essential and key step in any image processing (IP)-based techniques that improve the visual performance of an entire image. Various techniques are presented in this area which improves the quality of object in the image (Khan, Javed, Sharif, Saba, & Rehman, 2019).

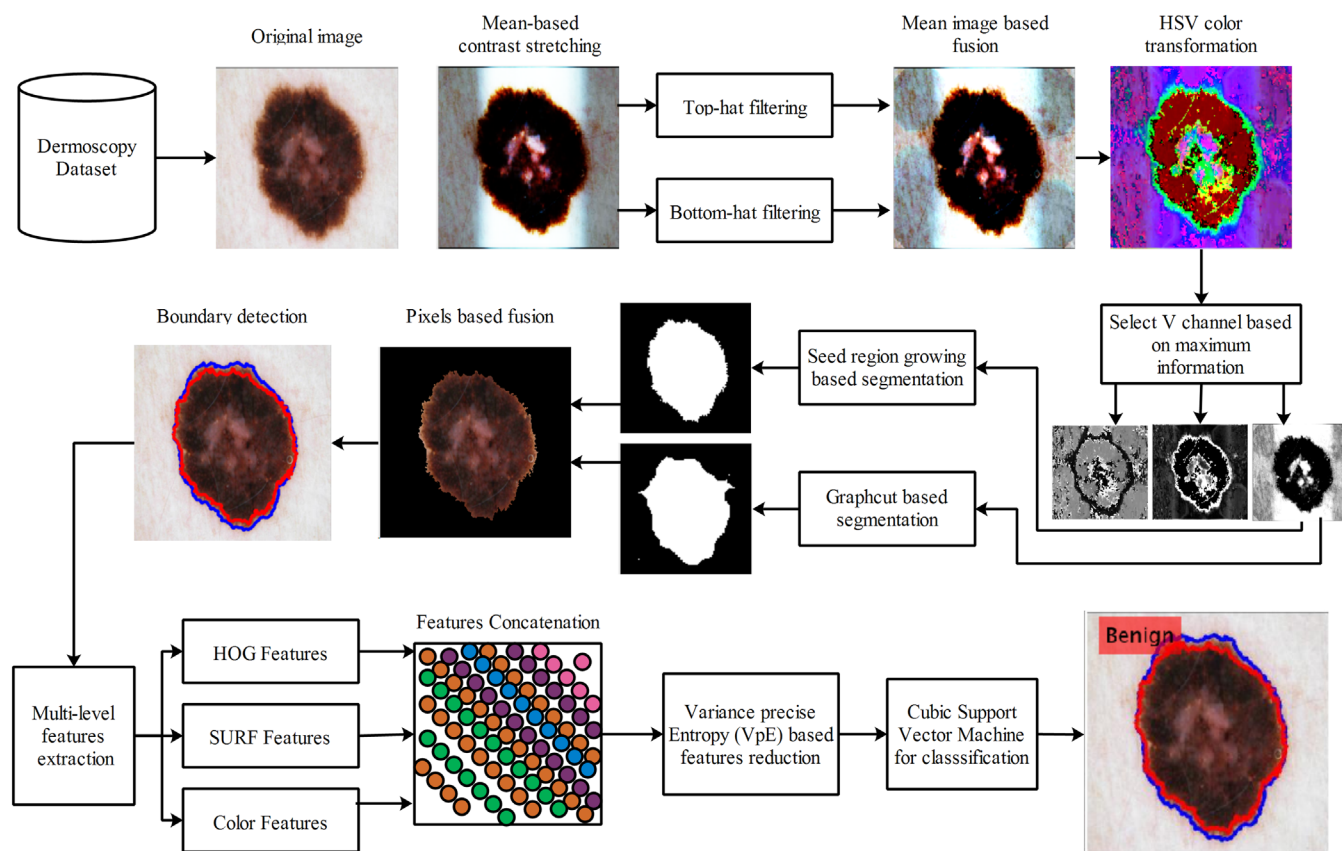


FIGURE 1 Proposed system diagram of an automated system for skin lesion detection and classification [Color figure can be viewed at wileyonlinelibrary.com]

In this work, a fusion-based contrast stretching approach is proposed. A two-step process is performed for this purpose, such as the implementation of a new contrast function based on the mean value, and second, filters bases fusion for contrast enhancement. The mean-based contrast function is implemented to increase the internal contrast of an image, which is mathematically expressed as follows:

Let $F(k, l)$ indicate an input image of dimension 256×256 and μ denotes the mean value of input image $F(k, l)$ which is calculated as follows:

$$\phi_T(k, l) = \frac{1}{\Delta F} \quad (1)$$

$$\Delta F = 1 + \frac{\mu}{F(k, l)^x}, \quad x = 7 \quad (2)$$

$$\mu = \frac{1}{MN} \sum_{k=1}^M \sum_{l=1}^N (F(k, l)) \quad (3)$$

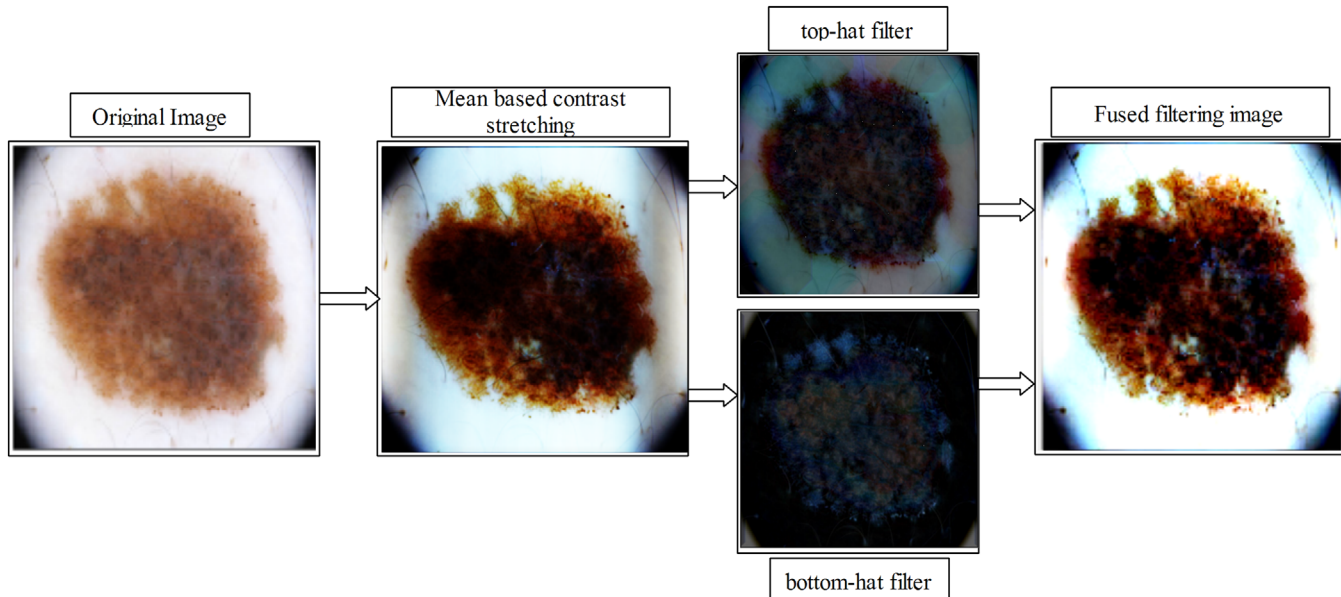


FIGURE 2 Filters fusion-based contrast stretching effects [Color figure can be viewed at wileyonlinelibrary.com]

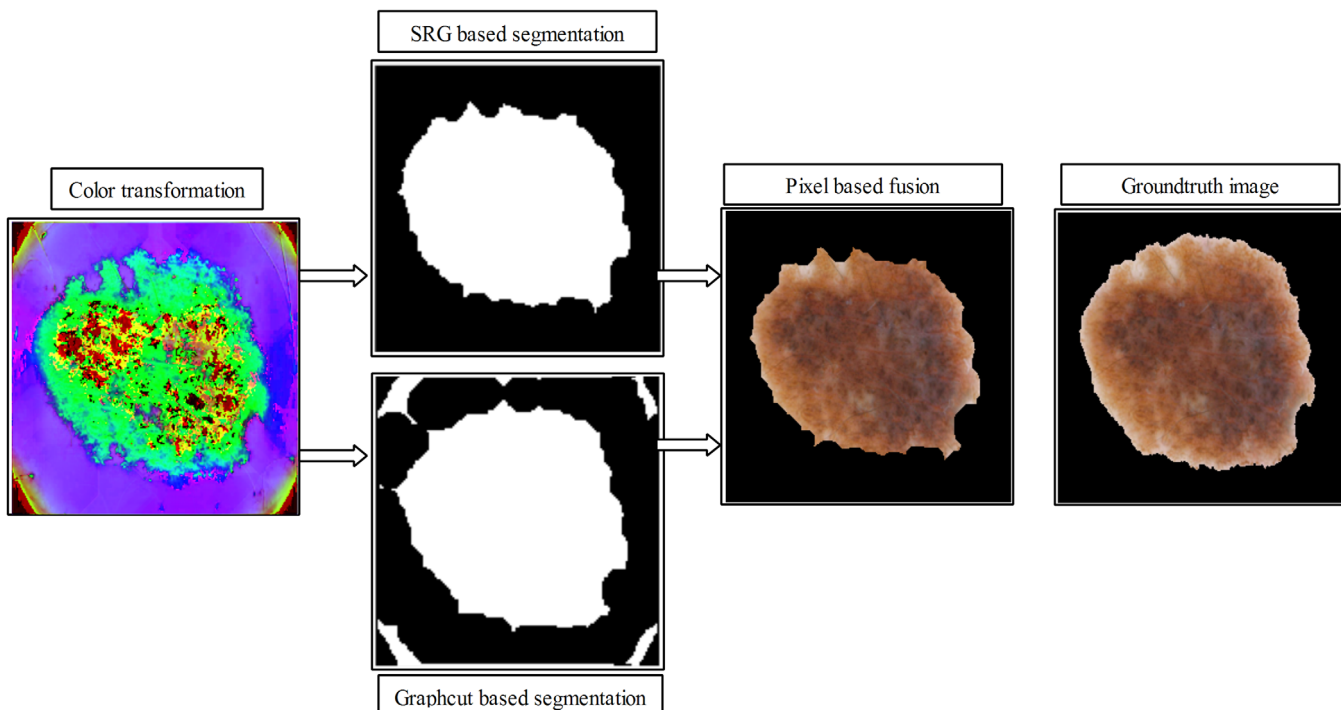


FIGURE 3 Proposed segmentation effects using a pixel-based fusion approach [Color figure can be viewed at wileyonlinelibrary.com]

where M and N denote the number of rows and columns pixels, $\phi_T(k, l)$ is a resultant mean-based contrast image, and x is a stretching element. The resultant mean-based contrast image $\phi_T(k, l)$ feed to top-hat and bottom-hat filters and fused their output by the following expression that returns a more precise image.

$$\phi_{Top}(k, l) = \phi_T(k, l) - (\phi_T(k, l) \cdot E) \quad (4)$$

$$\phi_{Bot}(k, l) = \phi_T(k, l) - (\phi_T(k, l) \cdot E) \quad (5)$$

where $\phi_{Top}(k, l)$ denotes the top-hat filtering image and $\phi_{Bot}(k, l)$ is a bottom hat filtering image, respectively, as shown in Figure 2. The output of both filtered images is fused as follows:

$$\phi_A'(k, l) = (\Delta_A(k, l) - \phi_{Bot}(k, l)) \quad (6)$$

$$\Delta_A(k, l) = \phi_{Top}(k, l) + \phi_T(k, l) \quad (7)$$

where the resultant fused image is $\phi_A'(k, l)$ of dimensional 256×256 . The effects are shown in Figure 2.

3.2 | Lesion segmentation

Skin lesion segmentation is an essential condition for an automated CAD system. Many techniques are available for lesion segmentation, but they have a tendency over and under segmentation because of few essential challenges such as hazy boundaries of a

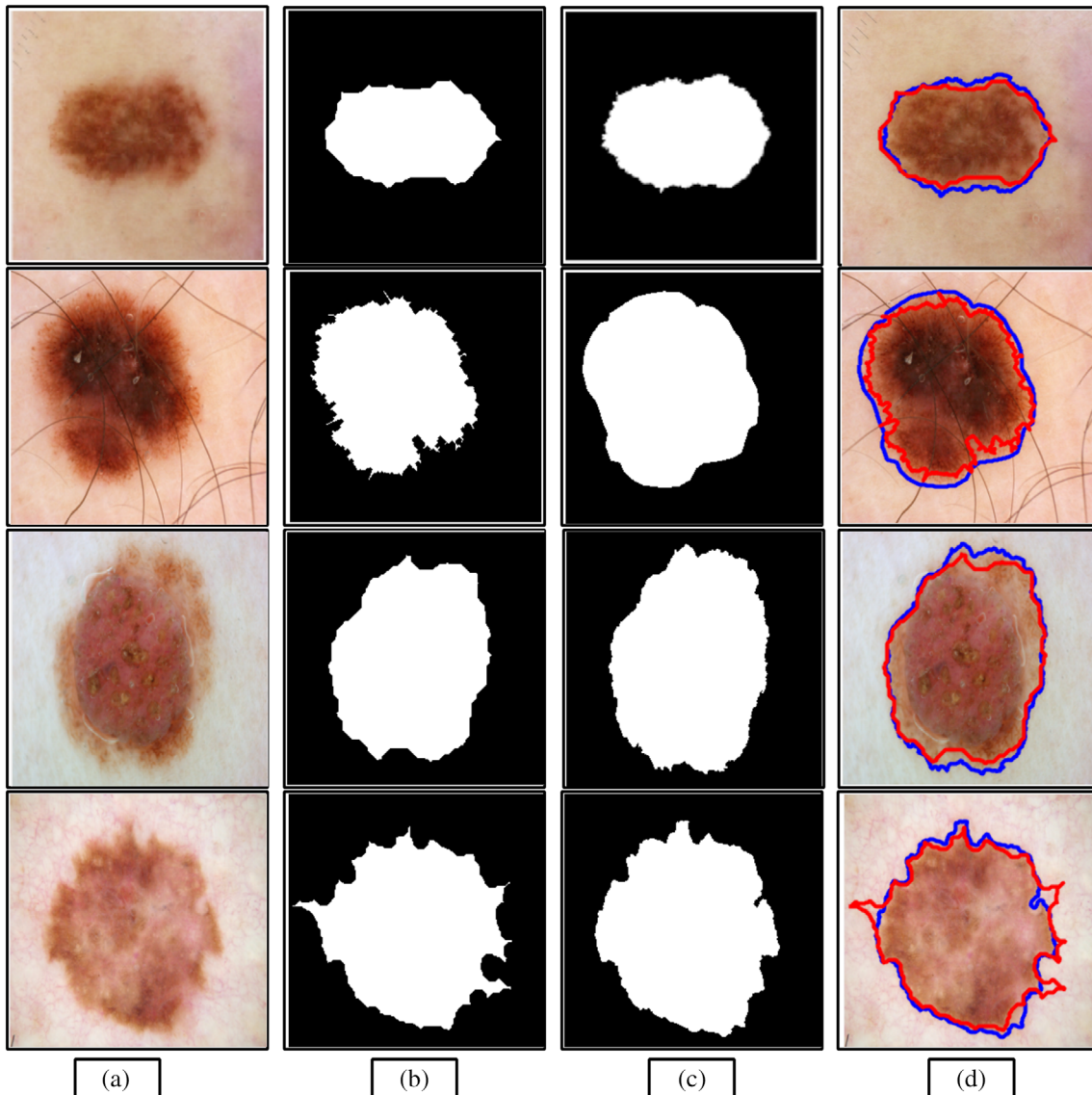


FIGURE 4 Proposed lesion segmentation effects. (a) Original image, (b) proposed fusion-based segmentation, (c) ground-truth image, and (d) boundary-based comparison. The red boundary denotes the proposed segmented image, whereas the blue line is the ground-truth region [Color figure can be viewed at wileyonlinelibrary.com]

lesion, presence of artifacts, and inhomogeneous textures. These problems affect the correct segmentation of lesions. Therefore, this work proposes a semiautomatic technique for lesion segmentation. The proposed method works in three substeps. In the first step, HSV color transformation is applied to the fused contrast stretch image. In the second step, HSV transformed image is feed to SRG and graph-cut-based segmentation methods, individually. The resultant segmented image of each method is fused by the pixel-based method for final output. The detailed description of each method simultaneously visible results is given in the following sections.

In the very first step, the HSV color transformation is performed and selects the best channel for an input of SRG-based segmentation. For this purpose, we select the V channel based on the maximum pixel's intensity information and feed to SRG. The SRG determines the number of pixels, edge map, extract important regions, and regions of the segmented area of an image. In this work, we utilized SRG for the extraction of the lesion region. In the SRG, the segmentation occurs with respect to the set of points, which are known as seeds. Let we have the seeds number start from S_1, S_2, \dots, S_n . By using Adams and Bischof (1994), SRG helps out in seeds selection, embedding the noise, irrelevant information, and also used to find the tessellation image regions that meet as a nonempty intersection S_i . After adding the pixel in the simple seeds set, the formulation of all unallocated pixels is formulated as follows:

$$W = \left\{ x \in \bigcup_{i=1}^n S_i \mid N(x) \cap \bigcup_{i=1}^n S_i \neq \emptyset \right\} \quad (8)$$

where W denotes the set of all unallocated pixel which has at least one border region, and $N(x)$ is a neighbor point of image pixel x and $x \in \phi_v$. Then compute the difference among $N(x)$ and region mean that are utilized for similarity measures. The mathematical formulation of this process is defined as follows:

$$\Delta(x) = |N(x) - \text{mean}(g(x))| \quad (9)$$

$$\text{mean}(x) = \frac{1}{n+1} \left[\Delta(x) = n \times \text{mean}_{x \in S_{i-1}}(x) \right] \quad (10)$$

where $g(x)$ show the gray value at point x and n denote the number of pixels of an image. This process is continued until no new neighbor is added to the region. Finally, we obtain a binary segmented image denoted by $\phi(S_i(k, l))$ and results are shown in Figure 3. Second, we utilized a well-known technique name graph-cut (Felzenszwalb & Huttenlocher, 2004) for lesion segmentation. The HSV transformed image is set as an input which we finally apply a threshold function and obtain a binary image denoted by $\phi(G_i(k, l))$ as shown in Figure 3.

In the last, we fused both segmented images using a pixel-based method, namely, PvMPMF. As we have two segmented images $\phi(S_i(k, l))$ and $\phi(G_i(k, l))$ of the same dimension 256×256 ,

each segmented image contains different pixels information of the same input image; therefore, through a fusion of both images, we can obtain a more informative image as individual segmented images. In the proposed PvMPMF approach, all information is fused, pixel by pixel. Mathematically, the fusion process is defined by the following expression:

$$\phi_{Fu}(k, l) = \sum_{i \in I_1} \sum_{j \in I_2} \left(p(I_1, I_2)(i, j) \log \frac{p(I_1, I_2)(i, j)}{pI_1(i)I_2(j)} \right) \quad (11)$$

where $I_1 \in \phi(S_i(k, l))$, $I_2 \in \phi(G_i(k, l))$, and $p(I_1, I_2)$ denote the joint probability mass function, and pI_1 , and pI_2 denote marginal probabilities of both segmented images. The output of this expression is a fused image as shown in Figure 3. The detailed segmentation results are given in Figure 4, which is compared with ground-truth images.

3.3 | Multilevel features extraction

In the area of pattern recognition, features play a key role in the classification process such as object classification (Raza et al., 2018), human action classification (Aurangzeb et al., 2019), medical diseases classification (Iqbal et al., 2019; Saba, Mohamed, El-Affendi, Amin, & Sharif, 2020, Saba, Mohamed, El-Affendi, Amin, & Sharif, 2020; Saba, Sameh, Khan, Shad, & Sharif, 2019), agriculture plants diseases recognition (Khan, Akram, Sharif, Awais, et al., 2018; Safdar et al., 2019), and many more (Khan et al., 2017; Sadad et al., 2018). In this work, we implement multilevel features extraction such as HOG, SURF, and color for the classification of skin lesions in the category of benign or malignant melanoma. The main purpose of multilevel feature extraction is to obtain the more precise information of skin lesions as compared to single feature type.

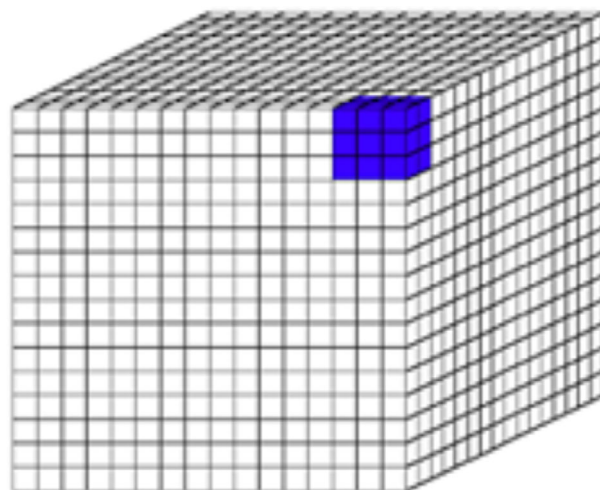


FIGURE 5 Blocks of video volume and blue area show 2×2 block in time, and 3×3 in space is used in descriptors [Color figure can be viewed at wileyonlinelibrary.com]

First, we extracted the HOG features from boundary extracted lesions. To extract the HOG, we need to compute gradient magnitude response either in horizontal or in a vertical direction. The two-dimensional vectors for each image are obtained. When θ orientation is equal to 8, the magnitude response is quantized. These responses are then aggregated in both spatial and temporal orders over pixel blocks. As shown in Figure 5, how an image is divided into several blocks. We have done interpolation between these blocks that is responsible for providing translation invariance to descriptors. Then, the magnitude responses are alienated in eight orientations that provide descriptors of 144 dimensions of HOG. After that, L_2 normalization is performed which means Euclidian distance among descriptors. The L_2 is defined as follows:

$$L_2 : f = \frac{\vec{v}}{\sqrt{\|\vec{v}\|_2^2 + e^2}} \quad (12)$$

After that, all responses of numerous adjacent blocks are concatenated. Finally, descriptors are normalized, and the feature vector of dimension $N \times 3780$ is returned.

Second, extracted features from lesion boundary images are SURF point features. SURF features served in four core steps: integral image generation, hessian detection, orientation descriptor assignment, and finally descriptor generation. To compute the surface integral pixels, an integral image is generated. Mathematically, the integrated image is computed as follows:

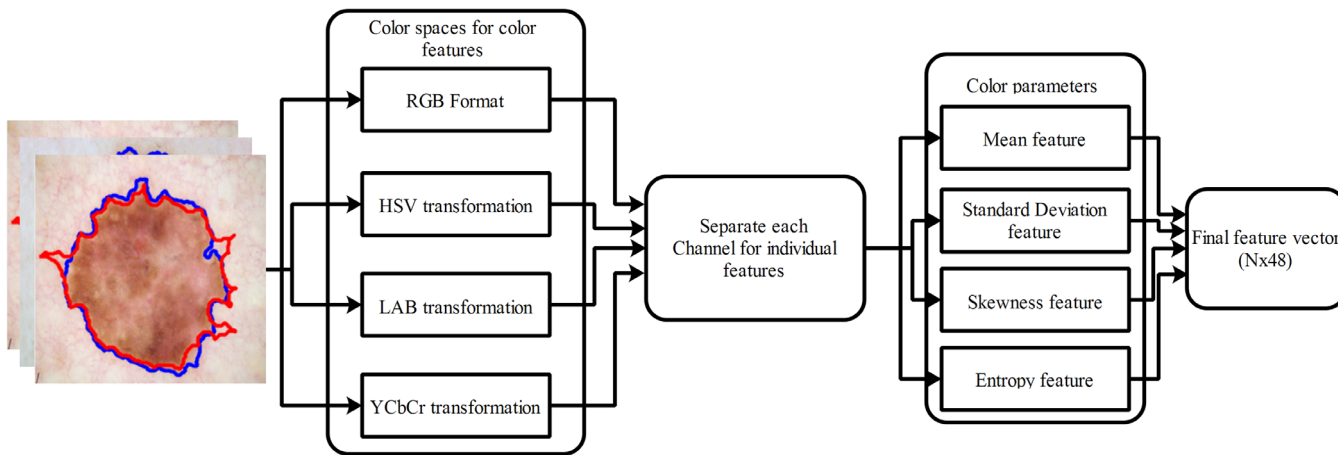


FIGURE 6 Flow of color feature extraction (Nasir et al., 2018) [Color figure can be viewed at wileyonlinelibrary.com]

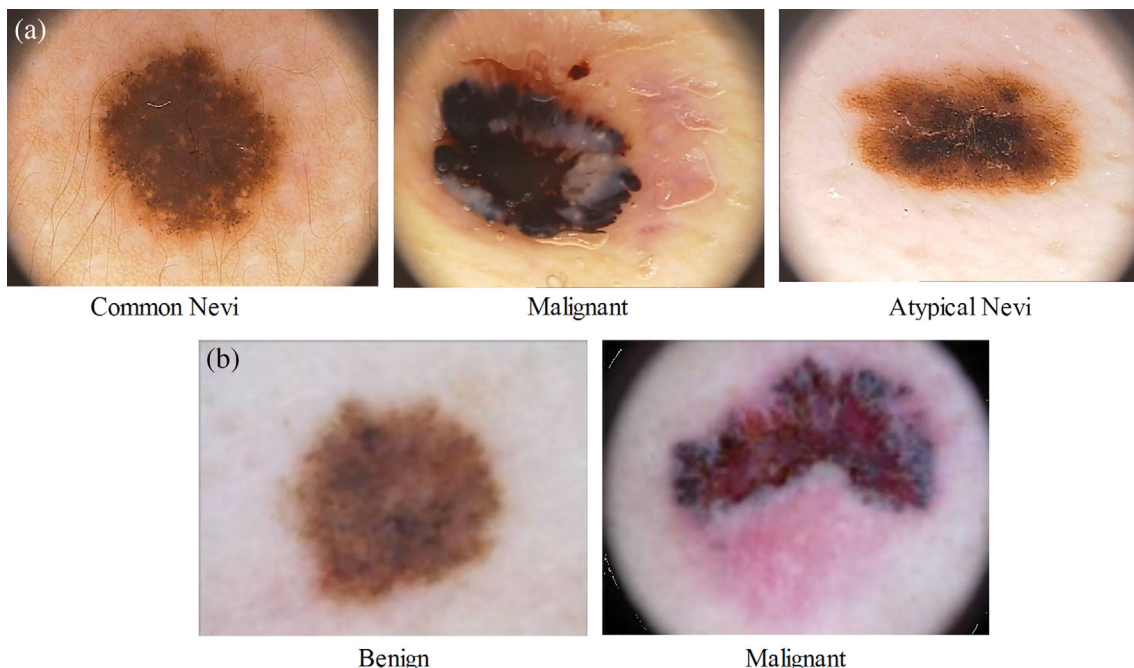


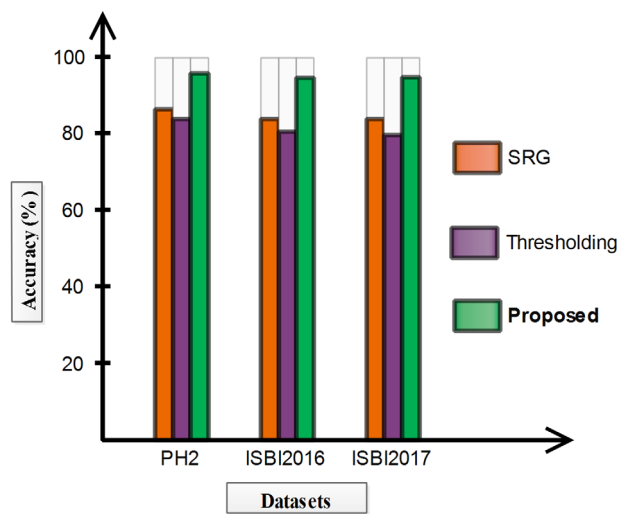
FIGURE 7 Sample dermoscopy images. (a) Images are selected from the PH2 dataset; (b) images are selected from ISBI2016 [Color figure can be viewed at wileyonlinelibrary.com]

TABLE 1 Proposed fusion-based segmentation performance for selected datasets

Dataset	Evaluation measures				
	Accuracy (%)	Sensitivity (%)	Precision (%)	FNR (%)	Time (s)
PH2	95.86	95.72	95.80	4.14	105.936
ISBI2016	94.79	93.26	93.40	5.21	276.790
ISIC2017	94.92	92.90	93.16	5.08	429.56

TABLE 2 Without fusion-based segmentation performance on selected datasets

Method	Segmentation technique		Evaluation measures			Time (s)
	SRG	Thresholding	Sensitivity (%)	Precision (%)	Accuracy (%)	
PH2	❖		87.24	86.24	86.52	74.690
		❖	84.90	82.10	83.96	79.990
ISBI2016	❖		86.59	83.51	83.94	117.886
		❖	83.46	79.49	80.62	110.902
ISIC017	❖		85.93	82.62	83.90	210.469
		❖	8.60	78.48	79.80	196.962

**FIGURE 8** Comparison of segmentation performance: fusion versus individual approach [Color figure can be viewed at wileyonlinelibrary.com]

$$I(r,s) = \sum_{k,l=0}^z \phi_{Fu}(k,l) \quad (13)$$

Then compute the hessian detector through the following Haar wavelet and Gaussian filter.

$$H(s,v) = \begin{bmatrix} \partial^2 g / \partial r^2 & \partial^2 g / \partial r \partial s \\ \partial^2 g / \partial r \partial s & \partial^2 f / \partial s^2 \end{bmatrix} \quad (14)$$

The SURF descriptors also compute the Hessian matrix to detect the interest points from the image based on square neighborhood points with the edge size. Mathematically, this expression is defined as follows:

$$\lambda(s) = T + \frac{\partial T^t}{\partial s} s + \frac{1}{2} s^t \frac{\partial^2 T}{\partial s^2} s \quad (15)$$

TABLE 3 Comparison of the proposed segmentation accuracy performance with recent methods on selected datasets

Method	Year	Accuracy (%)
PH2 dataset		
Afza et al. (2019)	2019	92.93
Bi et al. (2019)	2019	95.30
Bi et al. (2017)	2017	94.24
Proposed	2019	95.86
ISBI2016		
Pathan et al. (2018)	2018	94.6
Pennisi et al. (2016)	2016	91.18
Bozorgtabar, Sedai, Roy, and Garnavi (2017)	2017	92.3
Afza et al. (2019)	2019	93.98
Proposed	2019	94.79
ISBI2017 dataset		
Bi et al. (2019)	2019	94.08
Soudani and Barhoumi (2019)	2019	93.80
Proposed	2019	94.92

$$\hat{s} = \frac{\partial^2 T^{-1} \partial T}{\partial s^2} \quad (16)$$

$$\lambda(v) = T + \frac{\partial T^t}{\partial v} v + \frac{1}{2} v^t \frac{\partial^2 T}{\partial v^2} v \quad (17)$$

$$\hat{v} = \frac{\partial^2 T^{-1} \partial T}{\partial v^2} \quad (18)$$

In the third step, the rotation invariance is achieved by assigning each interest point a dominant direction and if no rotation is required, then skip orientation and assign a value (0,0). Finally, we obtain a SURF descriptor of dimension $N \times 64$, where N denotes

TABLE 4 Proposed skin lesion classification results using a different combination of features on PH2 dataset

Method	Features				Evaluation metrics			
	HOG	SURF	Color	Proposed	Recall (%)	Precision (%)	Accuracy (%)	FNR (%)
LSVM	❖				92.27	92.43	92.60	
		❖			90.38	90.79	90.36	
			❖		93.40	93.70	93.50	
				❖	95.28	95.76	95.69	
QSVM	❖				92.86	92.24	92.88	
		❖			91.49	91.30	91.56	
			❖		94.90	95.04	94.98	
				❖	96.72	96.94	96.90	
Cubic SVM	❖				94.95	96.24	95.96	
		❖			93.90	94.20	94.40	
			❖		97.56	97.98	97.90	
				❖	97.90	98.28	98.20	

Abbreviation: SVM, support vector machine.

the number of boundaries extracted images used for feature extraction.

In the last, we extracted color features by using an existing method (Nasir et al., 2018) and obtained a feature vector of dimension $N \times 48$. The flow of color feature extraction is shown in Figure 6.

These all features are finally concatenated in one matrix by using the following expression.

$$L_F(n_1) = \sum_{x_1}^A (\lambda_{\text{HOG}}(x_1)) \sum_{x_2}^B (\lambda_{\text{SURF}}(x_2)) \sum_{x_3}^C (\lambda_{\text{color}}(x_3)) \quad (19)$$

where the notation $L_F(n_1)$ denotes the length of a fused matrix which is the addition of three feature matrixes length such as $\lambda_{\text{HOG}}(x_1)$, $\lambda_{\text{SURF}}(x_2)$, and $\lambda_{\text{color}}(x_3)$ of dimensions $N \times 3780$, $N \times 64$, and $N \times 48$, respectively. Based on $L_F(n_1)$, size of the matrix is defined and combined as follows:

$$\lambda_{\text{fused}}(n_2) = [\lambda_{\text{HOG}}(x_1)_{N \times x_1}, \lambda_{\text{color}}(x_3)_{N \times x_3}, \lambda_{\text{SURF}}(x_2)_{N \times x_2}] \quad (20)$$

3.4 | Feature reduction and classification

In this work, we propose a VpE approach for the reduction of irrelevant features. The main motivation behind feature reduction is to minimize the prediction rate and computational time (Khan, Akram, Sharif, Javed, et al., 2018; Sharif et al., 2017). The proposed VpE approach processes in two different steps: variance calculation from the combined vector $\lambda_{\text{fused}}(n_2)$ and then the variance vector-based relative entropy (RE) is computed. The RE vector-based reduced negative and zero features. The variance of a vector $\lambda_{\text{fused}}(n_2)$ is computed as follows:

$$\text{var}(\lambda) = \frac{1}{MN} \sum_{r=1}^M \sum_{c=1}^N (\lambda_{rc}^2) - \mu^2 \quad (21)$$

where r and c denote the row and column features, respectively. This expression returns a variance feature vector of the same dimension which later feeds to RE for reduction of irrelevant information. Mathematically, the RE is defined as follows:

$$\text{RE}(r \mid c) = \sum_{r,c \in D} p(r,c) \ln \frac{p(r,c)}{q(r,c)} \quad (22)$$

Classically, the $p(r,c)$ shows the true observation while $q(r,c)$ represents the estimation value of $p(r,c)$. Finally, we set a threshold on the entropy vector and eliminate all negative and zero features. The remaining features which are nonzero and higher than zero are feed to cubic SVM (Jadhav, Ghontale, & Shrivastava, 2019) for final classification.

4 | EXPERIMENTAL SETUP AND RESULTS

The experimental process of the proposed method is done in two key steps. In the first step, segmentation-based evaluation is performed on three free available datasets such as PH2 (Mendonça, Ferreira, Marques, Marcal, & Rozeira, 2013), ISBI2016 (Gutman et al., 2016), and ISIC2017 (Codella et al., 2018). Ground-truth images are also freely available for these datasets as shown in Figure 7. The segmentation performance is evaluated by four performance measures like accuracy, sensitivity rate, precision rate, FNR, and segmentation time for the whole dataset. Second, in the classification phase, two freely available datasets, such as PH2 and ISBI2016, are utilized for the experimental process, as sample images are shown in Figure 7. All classification results are computed through a 50:50 approach via 10-fold cross-validation. The multiclass SVM via cubic kernel function is utilized for final classification accuracy and compared performance with LSVM and QSVM. MATLAB2018b is used for simulation by

Class	Classification Class		
	Common Nevi	Atypical Nevi	Melanoma
Common Nevi	94%	2%	3%
Atypical Nevi	3%	96%	1%
Melanoma	1%	4%	95%

(a)

Class	Classification Class		
	Common Nevi	Atypical Nevi	Melanoma
Common Nevi	92%	4%	4%
Atypical Nevi	3%	96%	1%
Melanoma			4% 94%

(b)

Class	Classification Class		
	Common Nevi	Atypical Nevi	Melanoma
Common Nevi	98%	2%	
Atypical Nevi	2%	98%	
Melanoma		4%	96%

(c)

Class	Classification Class		
	Common Nevi	Atypical Nevi	Melanoma
Common Nevi	99%		1%
Atypical Nevi		99%	1%
Melanoma	0.5%	2%	97.5%

(d)

FIGURE 9 Confusion matrices of cubic SVM for different feature types. (a) HOG features, (b) SURF features, (c) color features, and (d) proposed after reduction

using a Desktop Computer with 16GB of RAM. The IP MATLAB toolbox is utilized for feature extraction.

4.1 | Segmentation results

The proposed pixel matching fusion method for lesion segmentation is applied on three datasets individually, and results are computed in the form of sensitivity, precision, FNR, accuracy, and overall computation time, as elaborated in Table 1. Then, 95.86% accuracy rate is achieved using proposed fusion method on PH2 dataset whereas the other parameters are sensitivity (95.72%), precision (95.80%), FNR (4.14%), and computation time is 105.936 s. This noted time is for all 200 testing images. Second, the proposed fusion method achieves segmentation accuracy of 94.79% whereas the other parameter values are 93.26, 93.40, 5.21%, and 276.790 s. In the last, the obtain accuracy on the ISIC2017 dataset is 94.92% with other parameter values 92.90%, 93.16%, 5.08, and 429.56 s. The individual results on SRG and thresholding methods are also computed, given in Table 2. The results presented in Table 2 shows that the segmentation results are increased after the proposed fusion process. The accuracy-based comparison between fusion and individual techniques is also plotted in Figure 8. However, the fusion process increases the computation time which is a limitation of this approach. In the last, a comparison with existing techniques is also attained in Table 3 which shows that the proposed fusion approach outperforms as compared to current methods reported in state of the art.

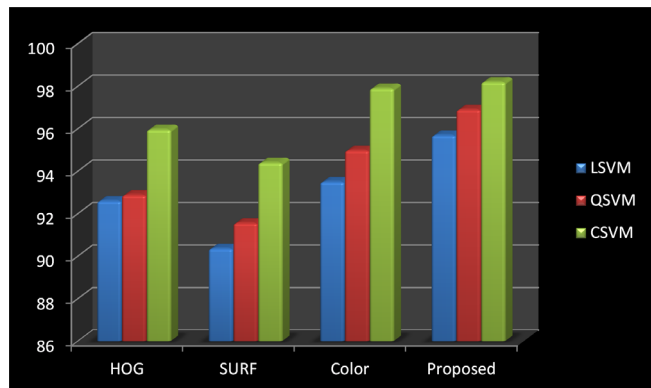


FIGURE 10 Comparison of segmentation performance: fusion versus individual approach [Color figure can be viewed at wileyonlinelibrary.com]

4.2 | Classification results

The classification results are evaluated on two freely available datasets: PH2 and ISBI2016. As mentioned earlier, the classification results are computed through 50:50 approaches via 10-fold cross-validation. Three kernel functions of multiclass SVM are utilized for accuracy measures such as linear, quadratic, and cubic. The performance of the cubic kernel function is outperforming as the other two kernels, and the results are given in Table 4. From Table 4, results are presented for all

TABLE 5 Proposed skin lesion classification results using a different combination of features on ISBI2016 dataset

Method	Features				Evaluation metrics			
	HOG	SURF	Color	Proposed	Recall (%)	Precision (%)	Accuracy (%)	FNR (%)
LSVM	❖				90.24	90.50	90.46	
		❖			87.04	87.84	87.62	
			❖		89.90	91.76	91.60	
				❖	90.40	93.70	93.49	
QSVM	❖				88.46	90.98	90.94	
		❖			82.16	85.24	85.06	
			❖		89.02	90.30	90.28	
				❖	90.00	92.31	92.09	
Cubic SVM	❖				90.94	93.70	93.69	
		❖			85.46	89.96	89.94	
			❖		90.60	93.88	93.76	
				❖	94.40	95.62	95.42	

Abbreviation: SVM, support vector machine.

Class	Classification Class	
	Melanoma	Benign
Melanoma	97%	3%
Benign	6%	94%

(a)

Class	Classification Class	
	Melanoma	Benign
Melanoma	93.5%	6.5%
Benign	14%	86%

(b)

Class	Classification Class	
	Melanoma	Benign
Melanoma	96%	4%
Benign	7.5%	92.5%

(c)

Class	Classification Class	
	Melanoma	Benign
Melanoma	97%	3%
Benign	6%	94%

(d)

individual and proposed VpE-based reduced features. The color features have individually achieved good accuracy when compared to the HOG and SURF patterns, but the fusion process increases almost 2–3% accuracy for PH2. The best achieve accuracy on the PH2 dataset is 98.20%, along with a recall rate of 97.90%, precision rate 98.28%, and FNR is 1.80%, respectively. The best accuracy of cubic SVM is 97.90%, which is achieved on color features. Using cubic kernel, the SVM accuracy for HOG and SURF features is 95.96 and 94.40%, respectively. The performance of cubic SVM is also verified through confusion matrices, given in Figure 9. Besides, the feature-based accuracy comparison is also conducted in Figure 10 which shows that the proposed automated system surpasses as a measure to individual feature vectors.

Table 5 shows the classification performance of the ISBI2016 dataset using individual feature vectors and proposed VpE-based reduced features. The linear, quadratic, and cubic kernel functions of SVM are utilized and achieve maximum accuracy of 95.42% for cubic SVM kernel function. For linear kernel function, the best achievable performance is 93.49% using the proposed VpE approach, whereas for quadratic function, the best accuracy is 92.09%. Overall, the cubic SVM outperforms and achieves accuracy of 93.69% for HOG features, 89.94% for SURF, and 93.76% for color. The accuracy performance of the CSVM is also verified in Figure 11. Moreover, a features-based comparison is also conducted in Figure 12, which gives the authenticity of the proposed VpE reduction approach.

FIGURE 11 Confusion matrices of cubic SVM for different feature types. (a) HOG features, (b) SURF features, (c) color features, and (d) proposed after reduction

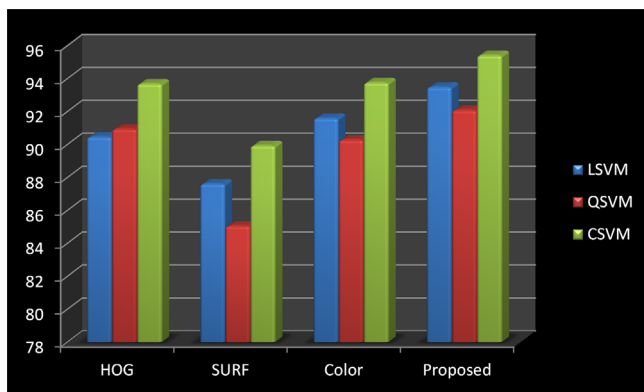


FIGURE 12 Features-based accuracy comparison using bar plots [Color figure can be viewed at wileyonlinelibrary.com]

TABLE 6 Proposed classification accuracy compared with recent methods on the same datasets

Method	Year	Accuracy (%)
PH2		
Satheesha, Satyanarayana, Prasad, and Dhruve (2017)	2017	97.00
Akram et al. (2018)	2018	97.50
Sharma and Bhave (2019)	2019	97.91
Proposed	2019	98.20
ISBI2016		
Khan et al. (2018))	2018	83.20
Yu, Chen, Dou, Qin, and Heng (2016)	2016	94.90
Yu et al. (2018)	2018	86.81
Khan, Akram, Sharif, Javed, et al. (2019) and Khan, Akram, Sharif, Saba, et al. (2019)	2019	89.20
Afza et al. (2019)	2019	93.80
Proposed	2019	95.42

Abbreviation: SVM, support vector machine.

4.3 | Comparative analysis

In the end, a comparison is conducted between the proposed classification accuracy and the recent method. The comparison is given in Table 6 for both datasets: PH2 and ISBI2016. The most recent methods utilized PH2 and ISBI2016 datasets for validation. To follow a few well-known methods, we compare our proposed classification accuracy with these performance parameters. Satheesha et al. (2017) introduced a computerized method for skin lesions recognition and evaluated on the PH2 dataset with achieved accuracy of 97%. The more recent, Akram et al. (2018) presented a saliency and traditional features-based approach for melanoma recognition and achieved an accuracy of 97.50%. In this method, they follow the process of different validations to analyze the method. Sharma and Bhave (2019) utilized the PH2 dataset for validation and achieved an improved

performance of 97.91%. In this work, we achieve an accuracy of 98.20% which is exceptional as compared to current methods.

Using ISIB016, Khan et al. (2018) presented an automated CAD system and achieved an accuracy of 83.20%. They also try to minimize the computational time of the classification process. Yu et al. (2018) improved the performance on the ISBI2016 dataset and accuracy reached 86.81%. The more recent, Khan, Akram, Sharif, Javed, et al. (2019) and Khan, Akram, Sharif, Saba, et al. (2019) introduced a fully automated system and evaluated on ISBI2016 dataset with an accuracy of 89.20%, which later improved by Afza et al. (2019) up to 93.80%. In this work, we achieve an accuracy of 95.42% on the ISBI2016 dataset, which is outstanding as compared to the current techniques.

5 | CONCLUSION

An automated system for melanoma detection and classification is presented in this work. Four primary steps are performed, such as contrast stretching, fusion-based lesion segmentation, multilevel feature extraction, and reduced by a new approach name VpE. The final features are classified by cubic SVM and achieve overall performance above 90% on PH2 and ISBI2016 datasets. The proposed system results show that the improvement in the lesion contrast pointedly helps in the segmentation step. Moreover, we also conclude from the fusion of the segmentation step; it increases the segmentation accuracy. Besides, the fusion process increases in the system computational time, but on the other side, it is meaningful increases in system accuracy. The problem of computation time is minimized through the reduction process, since the reduction process, minimizes the number of predictors. In the future, we will work on new optimization techniques using classical features. Moreover, the fusion of multiple classifiers is another interesting area of research that helps the researchers makes the systems more effective.

ACKNOWLEDGMENTS

This work was supported by Artificial Intelligence and Data Analytics (AIDA) Lab Prince Sultan University, Riyadh, Saudi Arabia. The authors are thankful for the support.

ORCID

Muhammad A. Khan  <https://orcid.org/0000-0001-7058-0715>

Zahid Mehmood  <https://orcid.org/0000-0003-4888-2594>

Tanzila Saba  <https://orcid.org/0000-0003-3138-3801>

REFERENCES

- Abbas, N., Saba, T., Mohamad, D., Rehman, A., Almazyad, A. S., & Al-Ghamdi, J. S. (2018). Machine aided malaria parasitemia detection in Giemsa-stained thin blood smears. *Neural Computing and Applications*, 29(3), 803–818.
- Abbas, N., Saba, T., Rehman, A., Mehmood, Z., Javaid, N., Tahir, M., ... Shah, R. (2019). Plasmodium species aware based quantification of malaria, parasitemia in light microscopy thin blood smear. *Microscopy Research and Technique*, 82(7), 1198–1214. <https://doi.org/10.1002/jemt.23269>

- Abbas, N., Saba, T., Rehman, A., Mehmood, Z., Kolivand, H., Uddin, M., & Anjum, A. (2019). Plasmodium life cycle stage classification based quantification of malaria parasitaemia in thin blood smears. *Microscopy Research and Technique*, 82(3), 283–295.
- Adams, R., & Bischof, L. (1994). Seeded region growing. *IEEE Transactions on Pattern Analysis and Machine Intelligence*, 16(6), 641–647.
- Afza, F., Khan, M. A., Sharif, M., & Rehman, A. (2019). Microscopic skin laceration segmentation and classification: A framework of statistical normal distribution and optimal feature selection. *Microscopy Research and Technique*, 82, 1471–1488.
- Akram, T., Khan, M. A., Sharif, M., & Yasmin, M. (2018). Skin lesion segmentation and recognition using multichannel saliency estimation and M-SVM on selected serially fused features. *Journal of Ambient Intelligence and Humanized Computing*, 1–20.
- Amin, J., Sharif, M., Yasmin, M., Saba, T., Anjum, M. A., & Fernandes, S. L. (2019). A new approach for brain tumor segmentation and classification based on score level fusion using transfer learning. *Journal of Medical Systems*, 43(11), 326.
- Amin, J., Sharif, M., Yasmin, M., Saba, T., & Raza, M. (2019). Use of machine intelligence to conduct analysis of human brain data for detection of abnormalities in its cognitive functions. *Multimedia Tools and Applications*. <https://doi.org/10.1007/s11042-019-7324-y>
- Aurangzeb, K., Haider, I., Khan, M. A., Saba, T., Javed, K., Iqbal, T., ... Sarfraz, M. S. (2019). Human behavior analysis based on multi-types features fusion and Von Nauman entropy based features reduction. *Journal of Medical Imaging and Health Informatics*, 9(4), 662–669.
- Cancer Facts and Figures 2019. American Cancer Society. <https://www.cancer.org/research/cancer-facts-statistics/all-cancer-facts-figures/cancer-facts-figures-2019.html>.
- Codella, N. C., Gutman, D., Celebi, M. E., Helba, B., Marchetti, M. A., Dusza, S. W., ... Kittler, H. (2018). Skin lesion analysis toward melanoma detection: A challenge at the 2017 international symposium on biomedical imaging (ISBI), hosted by the international skin imaging collaboration (ISIC). Paper presented at the 2018 IEEE 15th International Symposium on Biomedical Imaging (ISBI 2018).
- Dalila, F., Zohra, A., Reda, K., & Hocine, C. (2017). Segmentation and classification of melanoma and benign skin lesions. *Optik*, 140, 749–761.
- Ebrahim, A. Y., Kolivand, H., Rehman, A., Rahim, M. S. M., & Saba, T. (2018). Features selection for offline handwritten signature verification: State of the art. *International Journal of Computational Vision and Robotics*, 8(6), 606–622.
- Fahad, H. M., Khan, M. U. G., Saba, T., Rehman, A., & Iqbal, S. (2018). Microscopic abnormality classification of cardiac murmurs using ANFIS and HMM. *Microscopy Research and Technique*, 81(5), 449–457. <https://doi.org/10.1002/jemt.22998>
- Felzenszwalb, P. F., & Huttenlocher, D. P. (2004). Efficient graph-based image segmentation. *International Journal of Computer Vision*, 59(2), 167–181.
- Filali, I., & Belkadi, M. (2019). Multi-scale contrast based skin lesion segmentation in digital images. *Optik*, 185, 794–811.
- Gutman, D., Codella, N. C., Celebi, E., Helba, B., Marchetti, M., Mishra, N., & Halpern, A. (2016). Skin lesion analysis toward melanoma detection: A challenge at the international symposium on biomedical imaging (ISBI) 2016, hosted by the international skin imaging collaboration (ISIC). arXiv Preprint arXiv: 1605.01397.
- Husham, A., Alkawaz, M. H., Saba, T., Rehman, A., & Alghamdi, J. S. (2016). Automated nuclei segmentation of malignant using level sets. *Microscopy Research and Technique*, 79(10), 993–997. <https://doi.org/10.1002/jemt.22733>
- Iftikhar, S., Fatima, K., Rehman, A., Almazyad, A. S., & Saba, T. (2017). An evolution based hybrid approach for heart diseases classification and associated risk factors identification. *Biomedical Research*, 28(8), 3451–3455.
- Iqbal, S., Ghani Khan, M. U., Saba, T., Mehmood, Z., Javaid, N., Rehman, A., & Abbasi, R. (2019). Deep learning model integrating features and novel classifiers fusion for brain tumor segmentation. *Microscopy Research and Technique*, 82, 1302–1315.
- Iqbal, S., Ghani, M. U., Saba, T., & Rehman, A. (2018). Brain tumor segmentation in multi-spectral MRI using convolutional neural networks (CNN). *Microscopy Research and Technique*, 81(4), 419–427. <https://doi.org/10.1002/jemt.22994>
- Iqbal, S., Khan, M. U. G., Saba, T., & Rehman, A. (2017). Computer assisted brain tumor type discrimination using magnetic resonance imaging features. *Biomedical Engineering Letters*, 8(1), 5–28. <https://doi.org/10.1007/s13534-017-0050-3>
- Jadhav, A. R., Ghontale, A. G., & Shrivastava, V. K. (2019). Segmentation and border detection of melanoma lesions using convolutional neural network and SVM. In *Computational intelligence: Theories, applications and future directions-volume I* (pp. 97–108). NY USA: Springer.
- Jadooki, S., Mohamad, D., Saba, T., Almazyad, A. S., & Rehman, A. (2016). Fused features mining for depth-based hand gesture recognition to classify blind human communication. *Neural Computing and Applications*, 28 (11), 3285–3294. <https://doi.org/10.1007/s00521-016-2244-5>
- Jamal, A., Hazim Alkawaz, M., Rehman, A., & Saba, T. (2017). Retinal imaging analysis based on vessel detection. *Microscopy Research and Technique*, 80(17), 799–811. <https://doi.org/10.1002/jemt>
- Javed, R., Rahim, M. S. M., Saba, T., & Rehman, A. (2020). A comparative study of features selection for skin lesion detection from Dermoscopic images. *Network Modeling Analysis in Health Informatics and Bioinformatics*, 9(1), 1–4.
- Jianu, S. R. S., Ichim, L., & Popescu, D. (2019). Automatic diagnosis of skin cancer using neural networks. Paper presented at the 2019 11th International Symposium on Advanced Topics in Electrical Engineering (ATEE).
- Khan, M. A., Akram, T., Sharif, M., Javed, K., Rashid, M., & Bukhari, S. A. C. (2019). An integrated framework of skin lesion detection and recognition through saliency method and optimal deep neural network features selection. *Neural Computing and Applications*, 1–20.
- Khan, M. A., Akram, T., Sharif, M., Saba, T., Javed, K., Lali, I. U., ... Rehman, A. (2019). Construction of saliency map and hybrid set of features for efficient segmentation and classification of skin lesion. *Microscopy Research and Technique*, 82(6), 741–763.
- Khan, M. A., Akram, T., Sharif, M., Shahzad, A., Aurangzeb, K., Alhussein, M., ... Altamrah, A. (2018). An implementation of normal distribution based segmentation and entropy controlled features selection for skin lesion detection and classification. *BMC Cancer*, 18(1), 638.
- Khan, M. A., Javed, M. Y., Sharif, M., Saba, T., & Rehman, A. (2019). Multi-model deep neural network based features extraction and optimal selection approach for skin lesion classification. Paper presented at the 2019 International Conference on Computer and Information Sciences (ICCIS).
- Khan, M. A., Lali, I. U., Rehman, A., Ishaq, M., Sharif, M., Saba, T., ... Akram, T. (2019). Brain tumor detection and classification: A framework of marker-based watershed algorithm and multilevel priority features selection. *Microscopy Research and Technique*, 82(6), 909–922.
- Khan, M. A., Sharif, M., Javed, M. Y., Akram, T., Yasmin, M., & Saba, T. (2017). License number plate recognition system using entropy-based features selection approach with SVM. *IET Image Processing*, 12(2), 200–209.
- Majtner, T., Yildirim-Yayigz, S., & Hardeberg, J. Y. (2019). Optimised deep learning features for improved melanoma detection. *Multimedia Tools and Applications*, 78(9), 11883–11903.
- Majumder, S., & Ullah, M. A. (2019). Feature extraction from dermoscopy images for melanoma diagnosis. *SN Applied Sciences*, 1(7), 753.
- Marka, A., Carter, J. B., Toto, E., & Hassanpour, S. (2019). Automated detection of nonmelanoma skin cancer using digital images: A systematic review. *BMC Medical Imaging*, 19(1), 21.
- Mendonça, T., Ferreira, P. M., Marques, J. S., Marcal, A. R., & Rozeira, J. (2013). PH 2-A dermoscopic image database for research and benchmarking. Paper presented at the 2013 35th Annual International Conference of the IEEE Engineering in Medicine and Biology Society (EMBC).

- Mughal, B., Muhammad, N., Sharif, M., Rehman, A., & Saba, T. (2018). Removal of pectoral muscle based on topographic map and shape-shifting silhouette. *BMC Cancer*, 18, 778. <https://doi.org/10.1186/s12885-018-4638-5>
- Mughal, B., Muhammad, N., Sharif, M., Saba, T., & Rehman, A. (2017). Extraction of breast border and removal of pectoral muscle in wavelet. *Domain Biomedical Research*, 28(11), 5041–5043.
- Mughal, B., Sharif, M., Muhammad, N., & Saba, T. (2017). A novel classification scheme to decline the mortality rate among women due to breast tumor. *Microscopy Research and Technique*, 81, 171–180. <https://doi.org/10.1002/jemt.22961>
- Nasir, M., Attique Khan, M., Sharif, M., Lali, I. U., Saba, T., & Iqbal, T. (2018). An improved strategy for skin lesion detection and classification using uniform segmentation and feature selection based approach. *Microscopy Research and Technique*, 81(6), 528–543.
- Norouzi, A., Rahim, M. S. M., Altameem, A., Saba, T., Rada, A. E., Rehman, A., & Uddin, M. (2014). Medical image segmentation methods, algorithms, and applications. *IETE Technical Review*, 31(3), 199–213. <https://doi.org/10.1080/02564602.2014.906861>
- Pathan, S., Aggarwal, V., Prabhu, K. G., & Siddalingaswamy, P. (2019). Melanoma detection in dermoscopic images using color features. *Biomedical and Pharmacology Journal*, 12(1), 107–115.
- Pathan, S., Prabhu, K. G., & Siddalingaswamy, P. (2018). Hair detection and lesion segmentation in dermoscopic images using domain knowledge. *Medical & Biological Engineering & Computing*, 56(11), 2051–2065.
- Pathan, S., Prabhu, K. G., & Siddalingaswamy, P. (2019). Automated detection of melanocytes related pigmented skin lesions: A clinical framework. *Biomedical Signal Processing and Control*, 51, 59–72.
- Rahim, M. S. M., Norouzi, A., Rehman, A., & Saba, T. (2017). 3D bones segmentation based on CT images visualization. *Biomedical Research*, 28 (8), 3641–3644.
- Rahim, M. S. M., Rehman, A., Kurniawan, F., & Saba, T. (2017). Ear biometrics for human classification based on region features mining. *Biomedical Research*, 28(10), 4660–4664.
- Raza, M., Sharif, M., Yasmin, M., Khan, M. A., Saba, T., & Fernandes, S. L. (2018). Appearance based pedestrians' gender recognition by employing stacked auto encoders in deep learning. *Future Generation Computer Systems*, 88, 28–39.
- Rehman, A., Abbas, N., Saba, T., Mahmood, T., & Kolivand, H. (2018). Rouleaux red blood cells splitting in microscopic thin blood smear images via local maxima, circles drawing, and mapping with original RBCs. *Microscopic Research and Technique*, 81(7), 737–744. <https://doi.org/10.1002/jemt.23030>
- Rehman, A., Abbas, N., Saba, T., Mehmood, Z., Mahmood, T., & Ahmed, K. T. (2018). Microscopic malaria parasitemia diagnosis and grading on benchmark datasets. *Microscopic Research and Technique*, 81(9), 1042–1058. <https://doi.org/10.1002/jemt.23071>
- Rehman, A., Abbas, N., Saba, T., Rahman, S. I. U., Mehmood, Z., & Kolivand, K. (2018). Classification of acute lymphoblastic leukemia using deep learning. *Microscopy Research and Technique*, 81(11), 1310–1317. <https://doi.org/10.1002/jemt.23139>
- Saba, T. (2019). Automated lung nodule detection and classification based on multiple classifiers voting. *Microscopy Research and Technique*, 1–9. <https://doi.org/10.1002/jemt.23326>
- Saba, T., Al-Zahrani, S., & Rehman, A. (2012). Expert system for offline clinical guidelines and treatment. *Life Science Journal*, 9(4), 2639–2658.
- Saba, T., Bokhari, S. T. F., Sharif, M., Yasmin, M., & Raza, M. (2018). Fundus image classification methods for the detection of glaucoma: A review. *Microscopy Research and Technique*, 81, 1105–1121. <https://doi.org/10.1002/jemt.23094>
- Saba, T., Khan, M. A., Rehman, A., & Marie-Sainte, S. L. (2019). Region extraction and classification of skin cancer: A heterogeneous framework of deep CNN features fusion and reduction. *Journal of Medical Systems*, 43(9), 289.
- Saba, T., Khan, S. U., Islam, N., Abbas, N., Rehman, A., Javaid, N., & Anjum, A. (2019). Cloud-based decision support system for the detection and classification of malignant cells in breast cancer using breast cytology images. *Microscopy Research and Technique*, 82, 775–785. <https://doi.org/10.1002/jemt.23222>
- Saba, T., Mohamed, A. S., El-Affendi, M., Amin, J., & Sharif, M. (2020). Brain tumor detection using fusion of hand crafted and deep learning features. *Cognitive Systems Research*, 59, 221–230.
- Saba, T., Rehman, A., Mehmood, Z., Kolivand, H., & Sharif, M. (2018). Image enhancement and segmentation techniques for detection of knee joint diseases: A survey. *Current Medical Imaging Reviews*, 14(5), 704–715. <https://doi.org/10.2174/1573405613666170912164546>
- Saba, T., Sameh, A., Khan, F., Shad, S. A., & Sharif, M. (2019). Lung nodule detection based on ensemble of hand crafted and deep features. *Journal of Medical Systems*, 43(12), 332.
- Sadad, T., Munir, A., Saba, T., & Hussain, A. (2018). Fuzzy C-means and region growing based classification of tumor from mammograms using hybrid texture feature. *Journal of Computational Science*, 29, 34–45.
- Safdar, A., Khan, M. A., Shah, J. H., Sharif, M., Saba, T., Rehman, A., ... Khan, J. A. (2019). Intelligent microscopic approach for identification and recognition of citrus deformities. *Microscopy Research and Technique*, 82, 1542–1556.
- Satheesha, T., Satyanarayana, D., Prasad, M. G., & Dhruve, K. D. (2017). Melanoma is skin deep: A 3D reconstruction technique for computerized dermoscopic skin lesion classification. *IEEE Journal of Translational Engineering in Health and Medicine*, 5, 1–17.
- Sengupta, S., Mittal, N., & Modi, M. (2019). Improved skin lesion edge detection method using ant colony optimization. *Skin Research and Technology*.
- Sharif, M., Khan, M. A., Akram, T., Javed, M. Y., Saba, T., & Rehman, A. (2017). A framework of human detection and action recognition based on uniform segmentation and combination of Euclidean distance and joint entropy-based features selection. *EURASIP Journal on Image and Video Processing*, 89(1), 1–18.
- Sharma, M., & Bhave, A. (2019). Lesion classification using convolutional neural network. In *Soft computing and signal processing* (pp. 357–365). NY, USA: Springer.
- Sreelatha, T., Subramanyam, M., & Prasad, M. G. (2019). Early detection of skin cancer using melanoma segmentation technique. *Journal of Medical Systems*, 43(7), 190.
- Ullah, H., Saba, T., Islam, N., Abbas, N., Rehman, A., Mehmood, Z., & Anjum, A. (2019). An ensemble classification of exudates in color fundus images using an evolutionary algorithm based optimal features selection. *Microscopy Research and Technique*. <https://doi.org/10.1002/jemt.23178>
- Yousaf, K., Mehmood, Z., Saba, T., Rehman, A., Munshi, A. M., Alharbey, R., & Rashid, M. (2019). Mobile-health applications for the efficient delivery of health care facility to people with dementia (PwD) and support to their carers: A survey. *BioMed Research International*, 1–26.
- Yu, Z., Jiang, X., Zhou, F., Qin, J., Ni, D., Chen, S., ... Wang, T. (2018). Melanoma recognition in dermoscopy images via aggregated deep convolutional features. *IEEE Transactions on Biomedical Engineering*, 66(4), 1006–1016.

How to cite this article: Rehman A, Khan MA, Mehmood Z, Saba T, Sardaraz M, Rashid M. Microscopic melanoma detection and classification: A framework of pixel-based fusion and multilevel features reduction. *Microsc Res Tech*. 2020;83:410–423. <https://doi.org/10.1002/jemt.23429>